Journal of Petroleum Science and Engineering 157 (2017) 441–450

Contents lists available at ScienceDirect

Journal of Petroleum Science and Engineering

journal homepage: www.elsevier.com/locate/petrol

Mechanical entrapment analysis of enhanced preformed particle gels (PPGs) in mature reservoirs

Amir Farasat [a], Mohsen Vafaie Sefti [a,**], Saeid Sadeghnejad [b,*], Hamid Reza Saghafi [c]

[a] Department of Chemical Engineering, Faculty of Chemical Engineering, Tarbiat Modares University, Tehran, Iran
[b] Department of Petroleum Engineering, Faculty of Chemical Engineering, Tarbiat Modares University, Tehran, Iran
[c] IOR/EOR Research Institute, Tehran, Iran

ARTICLE INFO

Keywords:
Preformed particle gels
Mechanical entrapment
Gel particle-pore size ratio
Temperature
Fluid velocity
Experimental design

ABSTRACT

The injection of preformed particle gels (PPGs) is one of the novel solutions to improve conformance control in mature waterflooded reservoirs. In this method, the interaction between PPGs and pore structure controls the performance of the PPG solution in reservoir heterogeneity correction. Thus, the behavior evaluation of these deformable particles in eroded porous media, especially near the injection wells, is a key factor in designing and simulating conformance control treatments. In this study, a central composite design is used to propose a set of flooding experiments. Then, a comprehensive statistically based method is employed to assess the effects of some factors on the mechanical entrapment performance of PPGs in washouts and induced channels. Reservoir temperature as a new factor accompanied by some other factors, including displacing-fluid velocity and gel particle-pore size ratio is selected for experimental investigations. It is indicated that all nominated factors have a significant contribution with the importance order of reservoir temperature, gel particle-pore size ratio, and displacing fluid velocity.

The rising temperature and velocity cause the amount of entrapped PPGs to decrease, while gel particle-pore size ratio shows a relatively more complex behavior due to the viscoelastic nature of this product. It obeys quadratic behavior and the amount of entrapped PPGs is decreased gradually by increasing gel particle-pore size ratio and then increased dramatically. Finally, it is shown that the amount of entrapped PPGs can be predicted by using an accurate mathematical correlation. The results of this study can be used to guide the selection of best PPG size for successful water shut off under a particular reservoir condition.

1. Introduction

Induced fractures and high permeability channels, known as streaks or thief zones due to extensive long-term water flooding, are quite common in mature heterogeneous reservoirs (Bai et al., 2015). The heterogeneity of reservoirs is one of the key causes of conformance problem that lead to poor sweep efficiency, low hydrocarbon recovery, and excess water production. In these cases, the injected water follows the high permeable paths, leaving hydrocarbons in the low permeability zones untouched (Tongwa and Bai, 2014). Moreover, unwanted water production will cause problems such as additional water treatment, environmental and disposal concerns, and corrosion and scaling issues (Imqam et al., 2015).

Early excess water production and reservoir maturation are now forcing the oil and gas industry to focus on the cutting-edge EOR and conformance control methods to extend the duration life of mature reservoirs and produce more oil and gas from the enormous amount of hydrocarbons already bypassed (Abdulbaki et al., 2014; Ashrafizadeh et al., 2012; Tongwa and Bai, 2014). Therefore, water shut-off or controlling the flow direction of injected water is a significant environmental and financial challenge for the petroleum industry (Hu et al., 2016; Zhang et al., 2016). Conformance control is one of the enhanced oil recovery methods, which is defined as any approach that facilitates the movement of primarily un-swept remaining hydrocarbon and brings the production profile closer to a perfect conforming condition (Bai et al., 2015).

During the past years, many studies have been especially devoted to improving the conformance control methodologies (Chauveteau et al., 2003; Durán-Valencia et al., 2014; Elsharafi and Bai, 2013; Goudarzi et al., 2015; Imqam and Bai, 2015; Saghafi et al., 2016b; Sang et al.,

* Corresponding author.
** Corresponding author.
E-mail addresses: vafaiesm@modares.ac.ir (M. Vafaie Sefti), sadeghnejad@modares.ac.ir (S. Sadeghnejad).

http://dx.doi.org/10.1016/j.petrol.2017.07.028
Received 25 February 2017; Received in revised form 4 June 2017; Accepted 12 July 2017
Available online 13 July 2017
0920-4105/© 2017 Elsevier B.V. All rights reserved.

2014). Various materials have been introduced to decrease both water channeling, and high water cuts to enhance the oil recovery of mature oilfields (Imqam and Bai, 2015). Traditionally, in-situ polymer gel system has been one of the most applied technologies for conformance control and diverting flow during chase floods in fractured or heterogeneous reservoirs (Brattekås et al., 2016). Among polymeric gel systems, polyacrylamide gel has been the most prevalent one, which ensures adsorption on all rock minerals and makes a significant impact on water shut-off and profile control treatments (Bai et al., 2015; Chauveteau et al., 2003). However, there are some distinct disadvantages coupled with this technique, including the lack of gelation time control, shear degradation, dilution and gelant compositional changes when gels are in contact with reservoir minerals and fluids (Goudarzi et al., 2015; Imqam and Bai, 2015). Due to the aforementioned drawbacks, a new trend in gel treatments, i.e., Preformed Particle Gels (PPGs), has been developed for conformance control (Hu et al., 2016; Hua et al., 2013; Li et al., 2014; Yao et al., 2012). Preformed particle gels are expandable and hydrophilic polymer microgels that aim to tackle the problem of water channeling and poor sweep efficiency, by acting as in-depth diverting agents (Chen et al., 2015). The advantages of this technology over the in-situ gel placement methods are that: PPGs are formed in the surface before injection; therefore, the gelation process is not affected by the physicochemical condition of reservoir formation (Zhang et al., 2010, 2016). PPGs are insensitive to flow shear rate and strongly retaining into pore structures for long-term efficiency. They are size controlled with an arbitrary size distribution, small enough to make sure an in-depth treatment and large enough to considerably reduce water permeability as desired (Bai et al., 2007a, 2008; Bybee, 2005; Chauveteau et al., 2001, 2004; Feng et al., 2003; Hu et al., 2016; Saghafi et al., 2016a; Tang, 2007). These microgels are soft enough to be very easily collapsed by oil-water capillary pressure, so that reduce water permeability extremely while oil permeability is not affected (Bybee, 2005; Dupuis et al., 2016).

The field applications of PPGs have had very promising results (Bai et al., 2008, 2013a, 2013b; Liu et al., 2006). The performance of PPG treatment is influenced by the mechanisms of gel particles transporting through fractures and channels and the interactions between microgels and pore bodies (Chauveteau et al., 2004; Cozic et al., 2008; Dupuis et al., 2016). On the other hand, the phenomenological description and experimental investigation of the retention and movement of PPGs in porous media are also very complicated because of the deformability capability of these particles (Al-Ibadi and Civan, 2013). Thus, it is important to recognize how a PPG solution behaves during its propagation in pores and how environmental factors affect its performance. Extensive efforts have been made to consider the retention performance of some other types of microgels, like in-situ microgels and colloidal dispersion gels (CDGs), through fractures or high permeability media, both theoretically and experimentally (Choi et al., 2010; Feng et al., 2013; Guang et al., 2014; Spildo et al., 2010). Many experimental studies have been also devoted to specify the performance of PPG flooding in porous media (Goudarzi et al., 2015; Imqam and Bai, 2015; Imqam et al., 2016, 2017; Long, 2016; Sang et al., 2014; Tongwa and Bai, 2014; Zhang, 2014). However, to our knowledge, the retention evaluations of PPGs has not been evaluated in detail. The effect of particle elasticity on PPG retention was briefly examined by using two kinds of PPG (Wu and Bai, 2008). The results reveal that the soft PPGs have a lower retention than the hard ones. Moreover, the effect of flow shear rate and reservoir heterogeneity on the in-depth propagation and retention of PPGs through some sand packs were evaluated (Sang et al., 2014; Wang et al., 2012; Zhang, 2014). The results show that, as the flow rate increases, PPG can move into the deep area to achieve deep fluid diversion. Thus, the ultimate recovery factor is higher. Moreover, it was shown that the effect of PPG flooding on the sweep efficiency becomes more efficient in sand packs that are more heterogeneous.

The nature of retention of solid particles in porous media was evaluated by Gruesbeck and Collins. In their study, fine particles suspensions (glass beads) were injected into sand packs in which the average throat size of the pores had been determined. It was shown that when the ratio of particle diameter to throat size is less than 0.08 ($X = 0.08$), no significant plugging was observed, although particles could adsorb as a layer on the surface of the grains all over the porous media. At ratios from $X = 0.17$ to 0.25, both surface adsorption and plugging due to a "log-jam" phenomenon in the pore throats were detected. At ratios upper than 0.39, the particles made a filter cake on the face of the sand pack and no invasion was seen (Donaldson et al., 1989).

In contrast to solid particles, viscoelastic preformed particle gels can transport through pores due to their deformability (Cohen and Christ, 1986; Sorbie, 2013). Therefore, an additional category (i.e., mechanical entrapment) can be added to adsorption and log-jamming mechanisms (Bai et al., 2007b; Spildo et al., 2010). Mechanical entrapment happens in flow conduits that are narrow; thus gel particles with $X \geq 1$ can plug the throats or pass them by deforming under a threshold pressure drop across the pore throats (Bai et al., 2007b; Wang et al., 2013). This mechanism enables a more permeability reduction, which can leave a long-term increased resistance to flow in high permeability streaks and following water diversion effects (Saghafi et al., 2016a). Additionally, PPG compressibility reduces the residual oil saturation during its movement throughout porous media (Goudarzi et al., 2014; Wang et al., 2013). Therefore, the usage of PPGs with $X \geq 1$ is a beneficial choice for field applications and is investigated in this study.

The effects of temperature accompanied by some other variables such as PPG size, porous media permeability, and injection velocity on the mechanical entrapment of PPGs were not simultaneously investigated. Therefore, to gain more insights of PPG transport, some comprehensive experimental investigations, which are considered as essential supplements to theoretical studies, were conducted in this study to evaluate the in-depth propagation as well as mechanical entrapment properties of PPGs in various conditions. To better represent the porous media behavior, the rock samples were collected from a carbonate reservoir. In this case, limestone grain packs, which precisely model sharp-edged unconsolidated carbonate rocks, washouts and induced channels from both geometrical and PPG entrapment points of view, were used to perform the experiments. The main findings in these experiments can guide the selection of best PPG size for specific reservoirs and predict its performance.

The structure of this paper is as follows. The statistical and experimental approaches used in this study are explained in the next section. Then the results and a comprehensive discussion of the analysis are presented. This is followed by the conclusions and the key findings of this study.

2. Material and methods

2.1. Materials

2.1.1. Preformed particle gels

In harsh environments, PPGs undergo syneresis, which is due to hydrolysis of the amide groups and posterior ionic crosslinking with divalent cations in the water (Durán-Valencia et al., 2014). In addition, molecular structure degradation due to the thermal effect is also common (Ahmed, 2015; Caulfield et al., 2003; Dupuis et al., 2013; Van Vliet et al., 1991). Thus, the enhanced PPGs were recently presented for reservoirs up to a temperature of 145 °C and a water TDS of 225,000 mg/lit. These PPGs were formulated with 30 wt% of a 2:1:1:2 M ratio of four monomers of Acrylamide (AM), N, *N*-dimethyl acrylamide (DA), *N*-vinylpyrrolidone (NVP), and 2-acrylamido-2-methylpropane sulfonic sodium salt (AMPSNa). The N,N′ methylenebis (acrylamide) (MBA) with a weight percent of 0.55% was used as the cross-linker, and the mechanical properties of PPGs were enhanced by adding a 2.5 wt% of nano clay montmorillonite Na^+ (Saghafi et al., 2016a, 2016b). It was revealed that the mechanical properties of hydrogels could be considerably reinforced by adding nano clay (Darvishi et al., 2011; Gu and Ye, 2009; Yu et al., 2011). It was found that the swelling ratio of hydrogels reduced when the

concentration of nano clay montmorillonite Na^+, increased. Moreover, as the weight percentage of this clay increases, the syneresis resistance of gels improves in high temperature and salinity conditions (Durán-Valencia et al., 2014; Long, 2016; Saghafi et al., 2016b; Yu et al., 2011).

The weighed amount of montmorillonite Na^+ was dispersed into a certain quantity of distilled water by an ultrasonic disperser. Subsequently, specific amounts of AM, NVP, DA, AMPSNa monomers were successively poured into the container while the solution was stirred by a magnetic stirrer. Afterward, the nitrogen purging was begun, and the MBA was added to the solution. The solution mixing and nitrogen purging were continued for one hour, and then specific amounts of the Sodium persulfate initiator and N,N,N′, N'-tetramethylethylenediamine catalyst were added to the container. The polymerization was instantly commenced, and gel bulk was seen within several minutes. The gel held in distilled water for one day and then cut into parts and dried in a vacuum oven (Saghafi et al., 2016b). The product was crushed by a Fritsch ball mill and separated into different PPG sizes by test sieves from Haver & Beoker. In this study, the size ranges of 40–50 μm and 50–75 μm were used to prepare PPG solutions. A detailed view of the dried PPGs and the prepared PPG solution (40–50 μm) in distilled water at 25 °C is illustrated in Fig. 1.

The PPGs were swollen in distilled water with a concentration of 2500 ppm and placed in a mixing cell, which was set at the test temperature (i.e., 45, 70, or 95 °C). In order to have a homogenous PPG solution during flooding, a mixing cell was used.

2.1.2. Sand packs

The core samples of a carbonate oil reservoir were toluene cleaned by a Soxhlet extractor, crushed, and put through sieves. Then, the desired crushed particles (600–850 μm or 850–2000 μm) were used to pack a set of stainless steel tubes. The rock particles of known mass (M_R) were gently transferred to the slim tube while the tube was held on a vibrator. The vibrator placed the rock particles in a regular and sorted manner. In this situation, a rather homogenous sand pack was made. The mass of the sand pack, M_1, was measured by a 0.01-gr lab balance.

The tube fittings and ferrule sets were all from Swagelok. Moreover, the length, outer diameter, and wall thickness of tubes were 500, 9.525, and 0.889 mm, respectively.

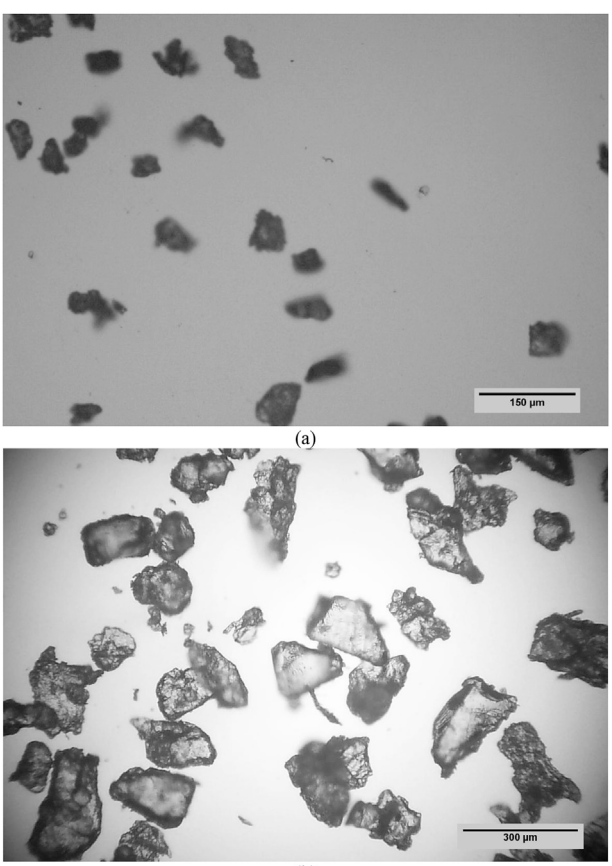

Fig. 1. Microscopic photos of (a) dried PPGs and (b) a PPG solution with the particle size range of 40–50 μm at 25 °C. Swelling process in distilled water causes the PPG size to increase around three times.

2.2. Experimental approach

2.2.1. Porosity and permeability of sand packs

The sand pack was vacuumed by a Corexport pump to a pressure of 0.005 Pa. Then, a Rosemount-3051 pressure transmitter was connected to the inlet of the sand pack to display the pressure. A precise Vinci dual positive displacement pump was used to saturate the sand pack with distilled water and increase its pressure to the atmospheric condition. The volume of the injected water was used to calculate the pore volume and porosity (Φ) of the sand pack. Afterward, by flooding the sand pack with various flow rates of distilled water, the permeability (K) was calculated.

2.2.2. Main experiments (mechanical entrapment)

After material preparation and calculation of the sand pack porosity and permeability, the following procedure was used to measure the mechanical entrapment of PPGs in porous media. The schematic of the experimental setup is shown in Fig. 2.

The sand pack was placed in an oven and connected to the pump and the mixing cell. The pump flow rate was set, and the sand pack was then flooded with 15 pore volumes of PPG solution. Afterward, the pump oven was set at desired temperature, and 15 pore volumes or more of distilled water with the similar flow rate were injected until no PPG was found in the discharge.

Finally, the sand pack was held in another oven at 120 °C for several days to be completely dried and its mass changes become zero (M_2). The difference between the initial mass of the sand pack before the flooding process (M_1) and final mass (M_2) showed the mass of the PPGs trapped in the porous media. The ratio of trapped PPG mass to the mass of rock particle gave the mechanical entrapment of PPGs in porous media (Eq. (1)).

$$C = \frac{M_2 - M_1}{M_R} \tag{1}$$

2.3. Design of experiments

To evaluate the effect of factors (and their interactions) like swelled particle size, fluid velocity, permeability, and temperature on the entrapment behavior of PPGs, the cost-effective statistical methods like the design of experiment (DOE) should be implemented. The three-level

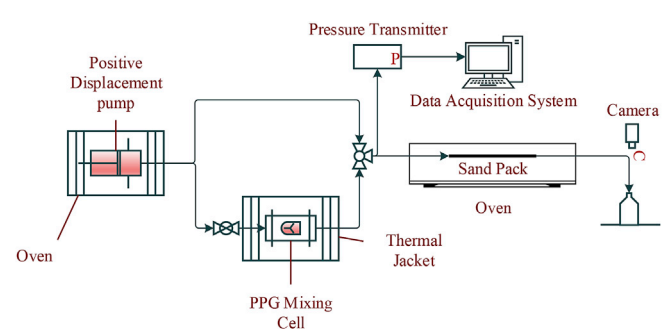

Fig. 2. Schematic of the experimental setup. Pump, PPG solution in mixing cell, and sand pack were held at test temperature. Data acquisition system was also used to display the inlet pressure over time.

Central Composite Design method was selected for this purpose. This method presents the shape of the entrapment response surface we are inspecting and provides excellent predictions over the entire design space. This approach comprises an enclosed factorial design with a center point that is augmented with a group of axial points that estimate the response curvature (Croarkin and Tobias, 2006).

However, by considering the relation between permeability and hydrodynamic pore diameter in Eq. (2) (Gruesbeck and Collins, 1982); swelled PPG size (D_1) and permeability were merged into one factor, i.e., gel particle-pore size ratio (D_{PT}), during our analysis (Eq. (3)).

$$D_{th} = 2 \times 1.15\sqrt{\frac{8K}{\phi}} \tag{2}$$

$$D_{PT} = \frac{D_1}{D_{th}} \tag{3}$$

Therefore, three factors including gel particle-pore size ratio, injection velocity, and temperature were used to construct a set of experiments. To select the operating bound of the factors, limitations of the implemented PPG material, field applications, and the experimental set up were considered. The injection flow rate was selected between 0.1 and 0.5 ml/min to meet the injection fluid velocity and regime around the wellbore in field applications. Thus, the flooding steps of each experiment lasted about 10–50 hours based on the designed flow rate. The temperature range was also designated between 45 and 95 °C to cover the thermal condition of reservoirs in various depths. The gel particle-pore size ratio was considered greater than one to investigate the mechanical entrapment mechanism and smaller than 2.5 to inject without plugging. The operating range of each factor and the proposed patterns of 15 entrapment experiments are shown in Table 1 and Table 2. The test temperatures and flow rates were set precisely, even though the gel particle-pore size ratio factor could not exactly set equal to the value suggested by the DOE. Therefore, the gel particle-pore size ratio proposed by DOE was changed to the nearest possible ratio.

Table 1
Factor constraints for design of experiments.

Factors	Unit	Min.	Mean	Max.
Flow rate	ml./min	0.1	0.3	0.5
Temperature	°C	45	70	95
$\frac{\text{PPG size}}{\text{Pore size}}$	dimensionless	1	1.75	2.5

Table 2
Matrix of experiments proposed by the central composite design method.

Experiment no.	Flow rate (ml./min)	Temperature (°C)	$\frac{\text{PPG size}}{\text{Pore size}}$
1	0.1	45	1
2	0.1	45	2.5
3	0.1	70	1.75
4	0.1	95	1
5	0.1	95	2.5
6	0.3	45	1.75
7	0.3	70	1
8	0.3	70	1.75
9	0.3	70	2.5
10	0.3	95	1.75
11	0.5	45	1
12	0.5	45	2.5
13	0.5	70	1.75
14	0.5	95	1
15	0.5	95	2.5

3. Results and discussion

For each experiment, the desired test conditions are shown in the DOE columns of Table 3. The appropriate porous media porosity, permeability, and the swelled PPG size should be selected to meet the proposed D_{PT} (Eq. (2) and Eq. (3)). Therefore, the proper size of dried PPG and its corresponding swelled size are revealed in the PPG columns (Farasat et al., 2017). The size of rock particles used in the sand pack and its porosity and permeability are shown in the sand pack columns as well. By using Eq. (2) and Eq. (3), the actual D_{PT} can be found.

All proposed experiments were run by the experimental approach explained in the previous section, and the results are shown in Table 3. The actual velocity of the fluid in the sand pack is also obtained from Eq. (4). The actual velocity as an intrinsic factor along with the actual D_{PT} and the test temperature will be used in the next subsection to find the proxy model of PPG entrapment. The detailed discussions about the effect of each factor on the entrapment will be presented later.

$$V = \frac{Q}{A\Phi} \tag{4}$$

3.1. Proxy model of entrapment

To construct the proxy model of PPG entrapment, the least squares method was used to fit the entrapment responses as a polynomial with the main three factors and all cross interaction terms. A simple saddle-shaped model (Eq. (5)) with an R^2 of 0.98 and adjusted R^2 of 0.94 was obtained which curved up in the direction of D_{PT} and V axes and down in the direction of T.

$$C = 4.647 \times D_{PT}^2 - 7.566 \times 10^{-4} \times T^2 - 8.467 \times 10^{-6} \times V^2 - 0.085 \times D_{PT} \times T - 0.031 \times D_{PT} \times V - 3.465 \times D_{PT} + 1.082 \times 10^{-3} \times T \times V + 0.040 \times T - 0.076 \times V + 13.305 \tag{5}$$

Although the model was shown to be highly significant, it should be tested if some factors can be assumed as negligible ones. Therefore, the sequential F-test was used to assess the sequential sum of square (Seq. SS) as each polynomial term was entered into the fit. In the sequential F-test approach, the factors which have great contributions in the model sum of square (269.67) and present probabilities less than the significance level of the test ($P < 0.05$) are considered as statistically important factors that affect the results. In other words, these factors are effective in the polynomial (Croarkin and Tobias, 2006; JMP and Proust, 2012). The result of this test confirms that the quadratic terms of temperature and velocity can be omitted without any considerable effects on the fitting quality (Table 4).

By ignoring the insignificant quadratic terms (V × V, T × T), a new robust model was constructed, and its quality of fitness is shown in Fig. 3 and Table 5. The structure of this simplified model is shown in Eq. (6).

$$C = 4.244 \times D_{PT}^2 - 0.083 \times D_{PT} \times T - 0.031 \times D_{PT} \times V - 2.200 \times D_{PT} + 1.082 \times 10^{-3} \times T \times V - 0.068 \times T - 0.077 \times V + 15.851 \tag{6}$$

3.2. Selection of significant factors

The selection of the most important factors was made based on the proposed equation (Eq. (6)). The coefficients used to fit the model reveal their statistical meanings. These coefficients are highly dependent on the factor scales, and they should be examined in a scale-invariant fashion. This means converting factor ranges from an arbitrary scale to a meaningful one. This was done by converting the factor ranges into −1 to 1.

Table 3
Results of 15 mechanical entrapment experiments designed in Table 2 by the central composite design method.

No.	DOE			PPG			Sand Pack				Result		
	Q	T	Proposed D_{PT}	Dried PPG size (μm)	Average size of dried PPG (μm)	Average size of swelled PPG (D_1)	Size of rock particle (μm)	Φ	K	Hydrodynamic pore size (D_{th}) (Eq. (2))	Actual D_{PT} (Eq. (3))	Fluid actual velocity (Eq. (4))	Entrapment (C) (Eq. (1))
1	0.1	45	1	40–50	45	173.8	850–2000	39.2	312.6	183.7	0.9	25.6	**9.25**
2	0.1	45	2.5	50–75	62.5	241.4	600–850	40.8	108.2	105.9	2.3	24.6	**20.05**
3	0.1	70	1.75	40–50	45	181.5	600–850	41.1	107.6	105.3	1.7	24.4	**7.61**
4	0.1	95	1	40–50	45	189.2	850–2000	39.9	324.4	185.5	1.0	25.1	**3.76**
5	0.1	95	2.5	50–75	62.5	262.8	600–850	41.4	109.5	105.8	2.5	24.2	**8.83**
6	0.3	45	1.75	40–50	45	173.8	600–850	40.3	106.1	105.6	1.6	74.6	**7.06**
7	0.3	70	1	40–50	45	181.5	850–2000	39.3	318.5	185.2	1.0	76.5	**5.3**
8	0.3	70	1.75	40–50	45	181.5	600–850	40.9	108.1	105.8	1.7	73.5	**6.12**
9	0.3	70	2.5	50–75	62.5	252.1	600–850	40.4	107.3	106.0	2.4	74.4	**10.85**
10	0.3	95	1.75	40–50	45	189.2	600–850	41.3	109.5	105.9	1.8	72.8	**3.23**
11	0.5	45	1	40–50	45	173.8	850–2000	39.7	322.7	185.5	0.9	126.3	**4.24**
12	0.5	45	2.5	50–75	62.5	241.4	600–850	41	110.2	106.7	2.3	122.3	**8.75**
13	0.5	70	1.75	40–50	45	181.5	600–850	40.7	108.8	106.4	1.7	123.2	**4.04**
14	0.5	95	1	40–50	45	189.2	850–2000	39.3	314.1	183.9	1.0	127.5	**1.84**
15	0.5	95	2.5	50–75	62.5	262.8	600–850	40.5	106.6	105.5	2.5	123.8	**4.26**

Table 4
Sequential F-test on primary model.

Source	DF	Seq. SS	F ratio	Prob.> F
T	1	75.24	60.7720	0.0006
D_{PT}	1	74.64	60.2899	0.0006
V	1	71.15	57.4666	0.0006
$D_{PT} \times D_{PT}$	1	14.17	11.4461	0.0196
V × T	1	12.72	10.2759	0.0238
V × D_{PT}	1	9.74	7.8690	0.0378
T × D_{PT}	1	8.69	7.0214	0.0454
V × V	**1**	**3.30**	**2.6661**	**0.1634**
T × T	**1**	**0.007**	**0.0057**	**0.9430**
Model	9	269.67		

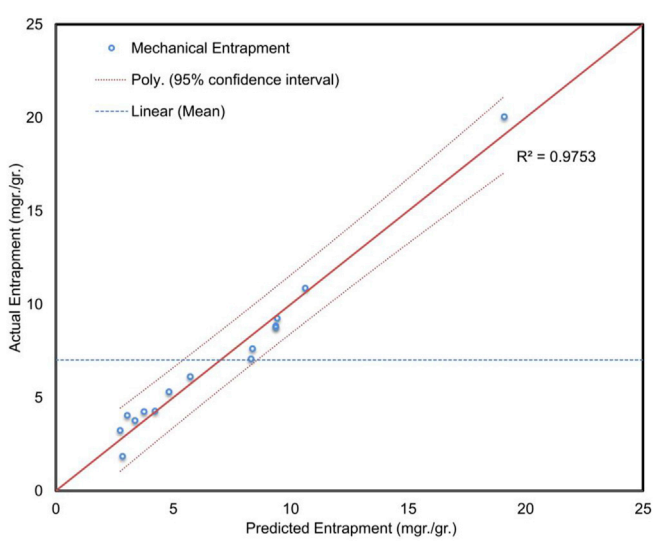

Fig. 3. Plot of actual entrapment versus predicted entrapment which shows a very good prediction whithin 95% confidence interval.

Table 5
Analysis of variance of entrapment model.

Model	Source	DF	SS	MS	F ratio	Prob.> F
C	Model	7	269.044	38.435	39.478	<0.0001
	Error	7	6.815	0.974		
	C. Total	14	275.859			

Furthermore, the coefficients should be transformed to be uncorrelated and identically distributed (JMP and Proust, 2012). Finally, the factors are sorted by the new coefficients in Fig. 4, showing the major effects at the top.

3.2.1. *Effect of temperature on entrapment*

The first important factor on entrapment is temperature. Its coefficient in the model is negative, and its increasing causes the entrapment to decrease. Furthermore, the negative dependence of the elastic modulus to temperature is observed in the cross-linked PAAm hydrogels (Li, 2009). The soft particles have lower entrapment potential in pores than the hard ones because they can easily pass pores-throats (Wu and Bai, 2008). By increasing the temperature from 45 to 95 °C, more swelling was observed, PPGs became softer; thus less entrapment was detected. It can also be approved by another argument wherein the resistance factor reduction caused by PPG solution in high-temperature condition is smaller than in low temperature (Saghafi et al., 2016a). The resistance factor is a measure of permeability reduction affected by entrapment, and its reduction is equivalent to entrapment reduction.

3.2.2. *Effect of gel particle-pore size ratio on entrapment*

Based on Fig. 4, the gel particle-pore size ratio (D_{PT}) is the second influential factor among others on mechanical entrapment. However, the gel particle-pore size ratio has a more complex effect on entrapment due

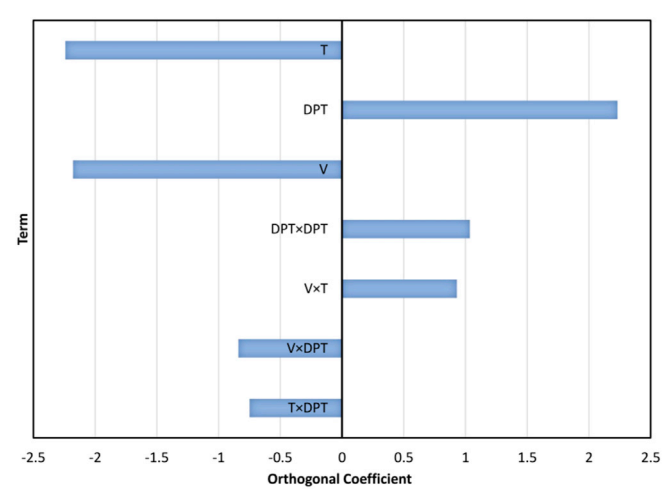

Fig. 4. Pareto plot showing the importance order of all nominated factors in the final entrapment model.

to the viscoelastic nature of PPG. It shows a quadratic behavior (D_{PT}^2) in Eq. (6), and the amount of entrapped PPGs is decreased gradually by increasing the gel particle-pore size ratio and then increased dramatically.

This dynamic shear stress-strain was measured by an Anton Paar rheometer at 25 °C (Fig. 5). The swelled PPG is remained in the elastic or linear viscoelastic region (constant storage modulus, G′) up to onset point of elastic to viscous phase change and shear strain of 0.1 (10%). Then, for larger strains (γ>10%), the microstructural collapsing starts; therefore, the rheological behavior of PPGs moves toward viscous phase, and they can be easily deformed (decreasing G', Fig. 5).

The shear strain can be calculated by Eq. (7) (Prentice, 1995). However, if it is supposed that d_2 is approximately perpendicular to the sides of the parallelogram, the Eq. (8) will be obtained (Fig. 6a).

$$\gamma = \tan(\psi) \tag{7}$$

$$\psi = \tan^{-1}(\gamma) \approx \cos^{-1}\left(\frac{d_2}{D_1}\right) \tag{8}$$

The PPG with gel particle-pore size ratio of greater than one should be placed under the shear stress of porous media until its diameter is reduced to pore throat diameter ($d_2 = D_{th}$) and passed throats (Fig. 6b and c). Based on this concept, spherical PPGs with diameters of only 0.6% greater than throat size (i.e., $D_{PT} = 1.006$) can pass throats in the elastic condition, and almost all applied PPGs (which have the D_{PT}>1.006) could pass throats under the viscous phase region (Eq. (9)). Therefore, by increasing PPGs' diameter (D_{PT}), the storage modulus of them decreases. Subsequently, PPGs becomes softer and the mechanical entrapment reduces.

$$\begin{aligned} &0.1 = \tan(\psi) \\ &\psi = \tan^{-1}(0.1) = 6^{\circ} \\ &6 \approx \cos^{-1}\left(\frac{d_2}{D_1}\right) \Rightarrow \frac{D_1}{d_2} \approx 1.006 \end{aligned} \tag{9}$$

In contrast, the shear strains of greater than unity (γ>100%, ψ > 45°) can break PPGs. At the shear strain of 100%, the strength modulus (G′) of PPGs is reduced to a tenth of its original value, so PPG rupturing occurs. The measurement of elongation at break (γ_e) is very much dependent upon testing geometry, condition, and dimension (Naficy et al., 2011). Most of the measurements are performed in tensile condition, which is different from one happened in a porous media and can be only used as an approximation (Gu and Ye, 2009). However, the tensile elongations at break of hydrogels containing montmorillonite Na^+ were reported to be approximately in the range of 100% (Gu and Ye, 2009; Noori et al., 2015). This observation shows that if the gel particle-pore size ratio rises to around 1.41, the PPG cannot pass through the pores by deformation

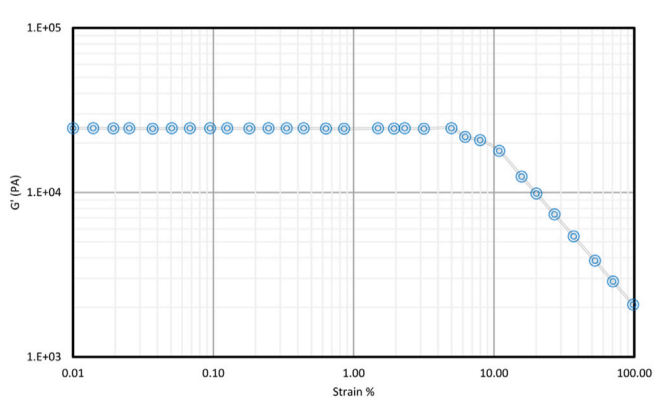

Fig. 5. Storage modulus of the hydrogel vs. shear strain at 25 °C. Hydrogel is remained in the elastic condition for strains less than 10%. Storage modulus decreases for strains greater than 10%.

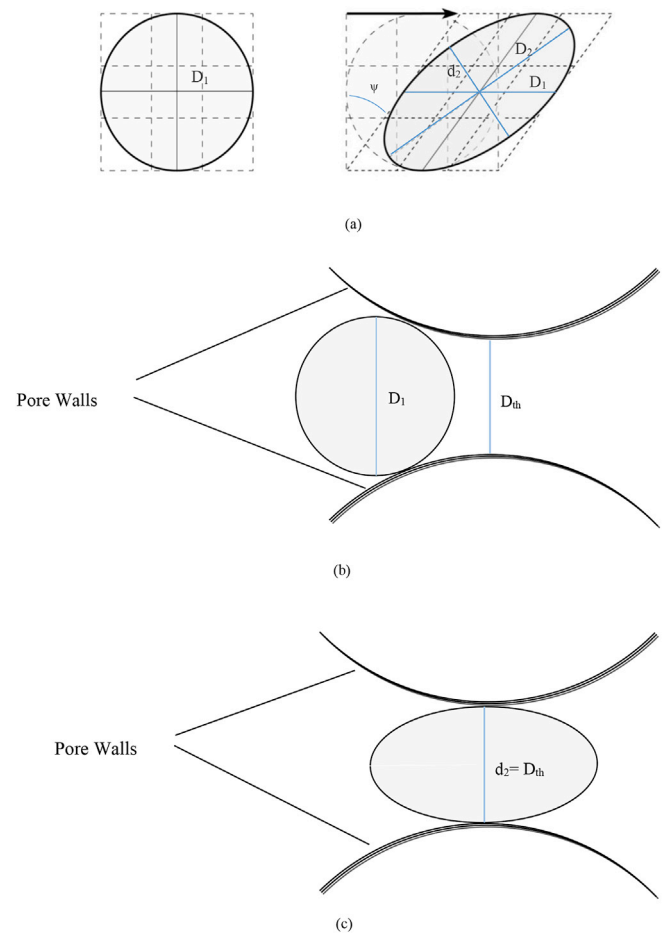

Fig. 6. PPG deformation in porous media. (a): Schematic of simple shearing process of a PPG. It shows that a circular PPG is reshaped to an ellipse under shear force. (b): Schematic of a PPG in a pore body. The diameter of PPG should be reduced to pass throat. (c): A deformed PPG in a throat.

mechanism and PPG breaking mechanism should be involved. Thus, the entrapment dramatically increases. This empirical argument is mainly supported by our test results (the quadratic term of D_{PT} in Eq. (6)) and will be shown in the subsection of checking interaction of factors (Fig. 9e and f).

The entrapment of a PPG in a pore throat is visualized by a SEM image in Fig. 7a. This photo is taken from a bunch of rock particles of the sand pack in the eighth experiment. The Fig. 7a shows that the PPGs can be stuck in the pore throats due to the roughness of the rock surfaces. This phenomenon can augment the effect of D_{PT} on the permeability reduction of porous media. Additionally, it is shown that the drying process makes the swelled PPGs to shrink and present some branchy shapes. The comparison of microscopic photos of PPG solution (Fig. 1) and the dried PPGs in a beaker has also confirmed this behavior (Fig. 8).

However, to visually investigate the effect of D_{PT} on the entrapment, the SEM images of rock particles in the three experiments of 7, 8, and 9 are revealed in Fig. 7. In these experiments, the test temperature and flow rate are identical, and the only variable was D_{PT}, which was changed from 1 to 2.5. These photos confirm the results of Table 3. The amount of trapped PPGs for D_{PT} of 1.75 is slightly greater than D_{PT} of 1, and the amount of trapped PPGs is intensely increased for the upper value of D_{PT}.

3.2.3. *Effect of velocity on entrapment*

Finally, the last important factor is injection velocity. At higher velocities, the drag force is the leading force among other forces in porous media (Zamani and Maini, 2009). Therefore, increasing velocity is equivalent to apply more drag force on particles from the carrier fluid.

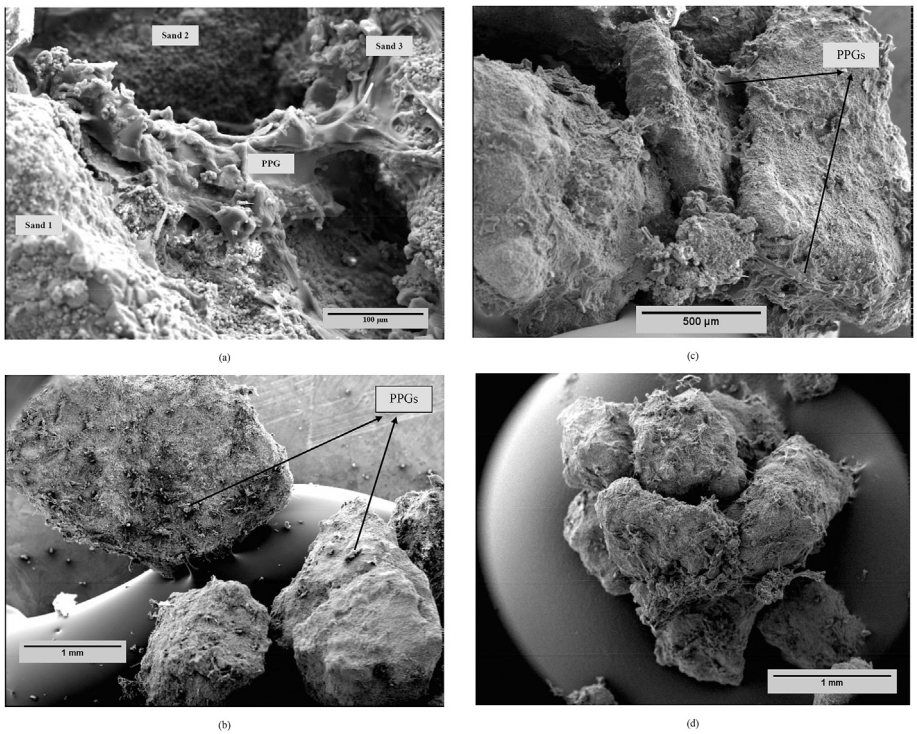

Fig. 7. Photos of dried PPGs in a porous media. (a): SEM photo of a trapped PPG in a throat (from experiment 8 in Table 3). The swelled PPG was retained in the pore throat and then dried during drying process. The dried PPG has a branchy shape. (b): SEM photo of rock particles in the experiment 7 ($D_{PT} = 1$). The stuck PPGs are shown on the rock walls as thready materials. Some of them are indicated by the arrows. (c): SEM photo of rock particles in the experiment 8 ($D_{PT} = 1.75$). This photo was taken from the rock particles shown in Fig. 7a. (d): SEM photo of rock particles in the experiment 9 ($D_{PT} = 2.5$). The PPGs are stuck on the rock walls, wherein, the rock particles are in contact with each other.

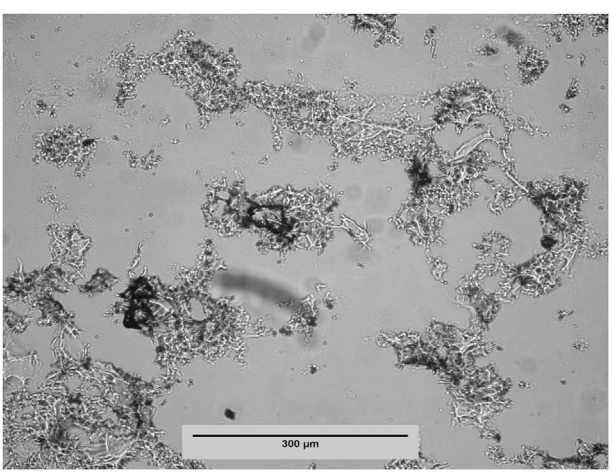

Fig. 8. Microscopic photo of dried PPGs. The drying process of swelled PPGs makes them to shrink and present some branchy shapes.

These forces can carry the PPGs deeper into the porous media and lower the entrapment (Ahfir et al., 2017). This is a preferred result for the regions near the injection well, which facilitates the in-depth conformance control process. Moreover, the shear-thinning behavior of PPG solution was also detected (Saghafi et al., 2016c). Thus at higher injection velocity, the solution has a lower effective viscosity so can be injected more easily.

3.2.4. Checking interaction of different factors

An interaction matrix can be used to demonstrate the interaction of row factors with column factors, and a line is plotted for each extremum of the row factor (Fig. 9). This matrix is symmetric for interaction evaluations. For example, Fig. 9a (or Fig. 9c) shows the interaction of velocity with temperature. In Fig. 9a, the amount of entrapment is shown by two lines at lowest and highest values of temperature versus velocity while the third factor (D_{PT}) remains at its mean level. Non-parallel lines give graphical evidence of possible interactions (JMP and Proust, 2012). However, the p-value of each term in the sequential F-test confirmed the existence of such interactions (Table 4).

Based on the matrix of interaction plots, the interaction between temperature and injection velocity has a significant effect on entrapment. The functionality of entrapment based on velocity is not identical at different levels of temperature (Fig. 9a). The entrapment is reduced by increasing fluid velocity. The slope of entrapment reduction can be more visible at lower temperatures, while its value is always greater than the values at higher temperature. This consequence can be confirmed by a reasoning that higher temperature sorely reduces the elasticity and threshold pressure of PPG; thus it can be propagated through porous media without important consideration of the carrying fluid velocity. A similar interpretation can be obtained from Fig. 9c. The entrapment can be significantly affected by temperature variation. At lower velocity (the red line in Fig. 9c) the temperature increase can soften PPGs; therefore, the particles can easily pass throats. Moreover, at higher fluid velocity, a stronger force is applied on the gel particles to penetrate throats regardless of the temperature level.

In addition, the effect of D_{PT} on entrapment change is more visible at low temperature and velocity conditions (Fig. 9e and f). Both plots of Fig. 9b and d show that the effects of V and T on entrapment are almost constant at the low level of D_{PT} (i.e., whether T and V are set at high or low levels). Nevertheless, at the high level of D_{PT}, the effects of T and V are more different based on their level. The smaller PPG needs lower differential pressure to pass the throats; hence, the entrapment at the lower level of D_{PT} is not significantly dependent on the velocity of the fluid. On the other hand, the entrapment at the high level of D_{PT} is substantially reliant on the applied force and rheological behavior of PPG, which are controlled by fluid velocity and reservoir temperature.

D_{PT} of 2.5 leads to a higher predicted entrapment than D_{PT} of one

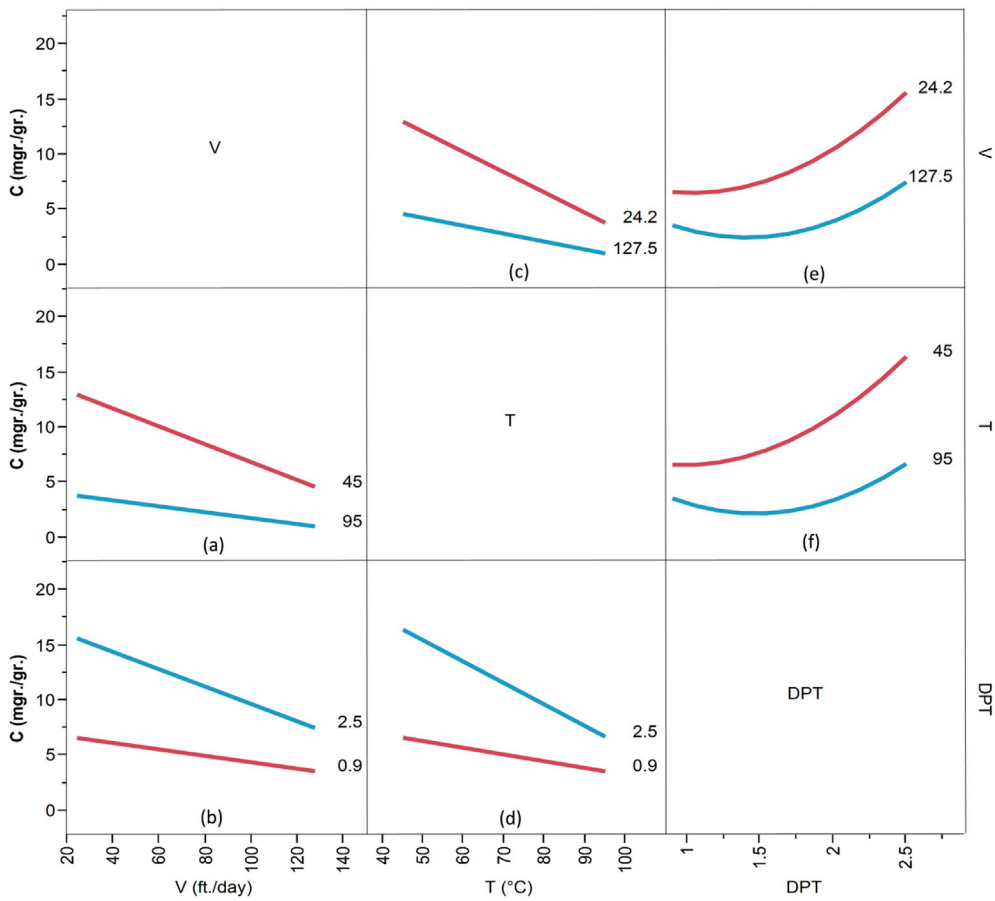

Fig. 9. The interaction plots of mechanical entrapment model.

(Fig. 9b and d). However, Fig. 9e and f show that there is a minimum in the D_{PT} curve. Initially, entrapment gradually decreases by increasing D_{PT}. The lowest possible entrapment was obtained at the highest temperature (95 °C) and injection velocity (127.5 ft/day) and D_{PT} equal to about 1.6 (Fig. 9f). Then, entrapment amount dramatically increases by increasing D_{PT}. These phenomena were investigated in the previous subsection (3.2.2) in detail. Higher PPG size will not always cause more entrapment due to the viscoelastic nature of PPGs.

4. Conclusions

1. The mechanical entrapment of PPGs in porous media is governed by reservoir temperature, gel particle-pore size ratio, and displacing fluid velocity.
2. The PPG entrapment decreases as the fluid velocity and reservoir temperature increase.
3. The fluid velocity in the near well regions is usually high to lower the PPG entrapment. Thus, the PPG solution can be effectively entered into the reservoir and can be used for in-depth conformance control.
4. The gel particle-pore size ratio shows a relatively more complex behavior due to the viscoelastic nature of this product. The amount of entrapped PPGs is decreased gradually by increasing the gel particle-pore size ratio and then increased dramatically.
5. There are strong two-level interactions between effective factors. The effect of velocity change on entrapment is more visible under low-temperature conditions and high gel particle-opening ratios. Moreover, the temperature change can greatly affect the entrapment, if the velocity and gel particle-opening ratio are set at low and high levels, respectively. In addition, the effect of D_{PT} change on entrapment is more detectable at low temperature and velocity conditions.
6. The amount of entrapped PPG can be estimated by an accurate mathematical correlation.

Acknowledgements

The authors wish to acknowledge the supports provided by the IOR/EOR Research Institute for this project.

Nomenclature

Item	Description	Unit
A	Cross-Sectional Area of Porous Media	cm. ^{2}
C	PPG Entrapment	mg. of PPGs/gr. of rock
d_2	Deformed PPG diameter	μm
D_1	PPG diameter	μm
D_2	Deformed PPG diameter	μm
D_{th}	Hydrodynamic Pore Diameter	μm
D_{PT}	Gel Particle- Pore Size Ratio	–
DF	Degree of Freedom	

(*continued on next page*)

(*continued*)

Item	Description	Unit
K	Permeability	Darcy
M_1	Mass of the Sand Pack before Flooding	gr.
M_2	Mass of the Sand Pack after Flooding	gr.
M_R	Mass of Rock Particles	gr.
Seq. SS	Sequential Sum of Square	
T	Temperature	°C
TDS	Total Dissolved Solid	mg./lit
Q	Flow Rate	ml./min
V	Actual velocity	ft./day (cm./min)
ψ	angular shear	°
γ	Shear strain	%
Φ	Porosity	%

References

Abdulbaki, M., Huh, C., Sepehrnoori, K., Delshad, M., Varavei, A., 2014. A critical review on use of polymer microgels for conformance control purposes. J. Petroleum Sci. Eng. 122, 741–753.

Ahfir, N.-D., et al., 2017. Porous media grain size distribution and hydrodynamic forces effects on transport and deposition of suspended particles. J. Environ. Sci. 53, 161–172.

Ahmed, E.M., 2015. Hydrogel: preparation, characterization, and applications: a review. J. Adv. Res. 6 (2), 105–121.

Al-Ibadi, A., Civan, F., 2013. Experimental investigation and correlation of treatment in weak and high-permeability formations by use of gel particles. SPE Prod. Operations 28 (04), 387–401.

Ashrafizadeh, M., Ahmad, R.S.A., Sadeghnejad, S., 2012. Improvement of polymer flooding using in-situ releasing of smart nano-scale coated polymer particles in porous media. Energy Explor. Exploitation 30 (6), 915–939.

Bai, B., Huang, F., Liu, Y., Seright, R.S., Wang, Y., 2008. Case Study on Preformed Particle Gel for In-depth Fluid Diversion. In: SPE Symposium on Improved Oil Recovery. Society of Petroleum Engineers.

Bai, B., et al., 2007a. Conformance control by preformed particle gel: factors affecting its properties and applications. SPE Reserv. Eval. Eng. 10 (4), 415–421.

Bai, B., Liu, Y., Coste, J.-P., Li, L., 2007b. Preformed particle gel for conformance control: transport mechanism through porous media. SPE Reserv. Eval. Eng. 10 (02), 176–184.

Bai, B., Wei, M., Liu, Y., 2013a. Field and lab experience with a successful preformed particle gel conformance control technology. In: SPE Production and Operations Symposium. Society of Petroleum Engineers.

Bai, B., Zhou, J., Liu, Y., Tongwa, P., 2013b. Thermo-dissoluble polymer for in-depth mobility control. In: International Petroleum Technology Conference.

Bai, B., Zhou, J., Yin, M., 2015. A comprehensive review of polyacrylamide polymer gels for conformance control. Petroleum Explor. Dev. 42 (4), 525–532.

Brattekås, B., Graue, A., Seright, R., 2016. Low-salinity chase waterfloods improve performance of Cr(III)-Acetate hydrolyzed polyacrylamide gel in fractured cores. SPE Reserv. Eval. Eng. 19 (02), 331–339.

Bybee, K., 2005. Rheology and transport in porous media of new water-shutoff/conformance-control microgels. J. Petroleum Technol. 57 (11), 71–72.

Caulfield, M.J., Hao, X., Qiao, G.G., Solomon, D.H., 2003. Degradation on polyacrylamides. Part II. Polyacrylamide gels. Polymer 44 (14), 3817–3826.

Chauveteau, G., et al., 2001. New size-controlled microgels for oil production. In: SPE International Symposium on Oilfield Chemistry. Society of Petroleum Engineers.

Chauveteau, G., et al., 2004. Disproportionate permeability reduction by soft preformed microgels. In: SPE/DOE Symposium on Improved Oil Recovery. Society of Petroleum Engineers.

Chauveteau, G., et al., 2003. In-depth permeability control by adsorption of soft size-controlled microgels. In: SPE European Formation Damage Conference. Society of Petroleum Engineers.

Chen, X., Feng, Q., Sepehrnoori, K., Goudarzi, A., Bai, B., 2015. Mechanistic modeling of gel microsphere surfactant displacement for enhanced oil recovery after polymer flooding. In: SPE/IATMI Asia Pacific Oil & Gas Conference and Exhibition. Society of Petroleum Engineers.

Choi, S.K., Sharma, M.M., Bryant, S., Huh, C., 2010. Ph-sensitive polymers for novel conformance-control and polymer-flood applications. SPE Reserv. Eval. Eng. 13 (06), 926–939.

Cohen, Y., Christ, F.R., 1986. Polymer retention and adsorption in the flow of polymer solutions through porous media. SPE Reserv. Eng. 1 (02), 113–118.

Cozic, C., Rousseau, D., Tabary, R., 2008. Broadening the application range of water shutoff/conformance-control microgels: an investigation of their chemical robustness. In: SPE Annual Technical Conference and Exhibition. Society of Petroleum Engineers.

Croarkin, C., Tobias, P., 2006. NIST/SEMATECH e-handbook of statistical methods. NIST/SEMATECH. July. Available online. http://www.itl.nist.gov/div898/handbook.

Darvishi, Z., Kabiri, K., Zohuriaan-Mehr, M., Morsali, A., 2011. Nanocomposite super-swelling hydrogels with nanorod bentonite. J. Appl. Polym. Sci. 120 (6), 3453–3459.

Donaldson, E.C., Chilingarian, G.V., Yen, T.F., 1989. Microbial Enhanced Oil Recovery, 22. Newnes.

Dupuis, G., Al-Maamari, R.S., Al-Hashmi, A.A., Al-Sharji, H.H., Zaitoun, A., 2013. Mechanical and thermal stability of polyacrylamide-based microgel products for EOR. In: SPE International Symposium on Oilfield Chemistry. Society of Petroleum Engineers.

Dupuis, G., Lesuffleur, T., Desbois, M., Bouillot, J., Zaitoun, A., 2016. Water conformance treatment using SMG microgels: a successful field case. In: SPE EOR Conference at Oil and Gas West Asia. Society of Petroleum Engineers.

Durán-Valencia, C., et al., 2014. Development of enhanced nanocomposite preformed particle gels for conformance control in high-temperature and high-salinity oil reservoirs. Polym. J. 46 (5), 277–284.

Elsharafi, M.O., Bai, B., 2013. Effect of strong preformed particle gel on unswept oil zones/areas during conformance control treatments. In: EAGE Annual Conference & Exhibition Incorporating SPE Europec. Society of Petroleum Engineers.

Farasat, A., Vafaie Sefti, M., Sadeghnejad, S., Saghafi, H.R., 2017. Effects of reservoir temperature and water salinity on the swelling ratio performance of enhanced preformed particle gels. Korean J. Chem. Eng. 34 (5), 1509–1516.

Feng, Q., Chen, X., Zhang, G., 2013. Experimental and numerical study of gel particles movement and deposition in porous media after polymer flooding. Transp. Porous Med. 97 (1), 67–85.

Feng, Y., et al., 2003. Characteristics of microgels designed for water shutoff and profile control. In: International Symposium on Oilfield Chemistry. Society of Petroleum Engineers.

Goudarzi, A., et al., 2014. New experiments and models for conformance control microgels. In: SPE Improved Oil Recovery Symposium. Society of Petroleum Engineers.

Goudarzi, A., et al., 2015. A laboratory and simulation study of preformed particle gels for water conformance control. Fuel 140, 502–513.

Gruesbeck, C., Collins, R.E., 1982. Entrainment and deposition of fine particles in porous media. Soc. Petroleum Eng. J. 22 (06), 847–856.

Gu, Y., Ye, L., 2009. Study on the polyvinylalcohol/montmorillonite composite hydrogel. Polymer-Plastics Technol. Eng. 48 (6), 595–601.

Guang, Z., Caili, D., Mingwei, Z., 2014. Investigation of the profile control mechanisms of dispersed particle gel. PLoS One 9 (6), e100471.

Hu, L., et al., 2016. Rheology properties and plugging performance of fluorescent polyacrylamide microspheres in fractures. J. Dispersion Sci. Technol. 37 (3), 345–351.

Hua, Z., et al., 2013. Study on plugging performance of cross-linked polymer microspheres with reservoir pores. J. Petroleum Sci. Eng. 105, 70–75.

Imqam, A., Bai, B., 2015. Optimizing the strength and size of preformed particle gels for better conformance control treatment. Fuel 148, 178–185.

Imqam, A., Bai, B., Wei, M., Elue, H., Muhammed, F.A., 2016. Use of hydrochloric acid to remove filter-cake damage from preformed particle gel during conformance-control treatments. SPE Prod. Operations 31 (03), 247–257.

Imqam, A., Goudarzi, A., Delshad, M., Bai, B., 2015. Development of a mechanistic numerical simulator for preformed particle gel applications in non-crossflow heterogeneous reservoirs. In: SPE Annual Technical Conference and Exhibition. Society of Petroleum Engineers.

Imqam, A., Wang, Z., Bai, B., 2017. The plugging performance of preformed particle gel to water flow through large opening void space conduits. J. Petroleum Sci. Eng. 156, 51–61.

JMP, A., Proust, M., 2012. Modeling and Multivariate Methods. SAS Institute.

Li, H., 2009. Smart hydrogel modelling. Smart Hydrogel Modelling Berlin Heidelberg. Springer (Berlin, Heidelberg).

Li, J., Liu, Y., Na, Z., Zeng, Z., Jiang, H., 2014. Investigation on the adaptability of the polymer microspheres for fluid flow diversion in porous media. J. Dispersion Sci. Technol. 35 (1), 120–129.

Liu, H., Han, H., Li, Z., Wang, B., 2006. Granular-polymer-gel treatment successful in the daqing oilfield. SPE Prod. Operations 21 (01), 142–145.

Long, Y., 2016. STUDY and Development of Robust Preformed Particle Gels for Conformance Control. Master Theses. Missouri University of Science and Technology.

Naficy, S., Brown, H.R., Razal, J.M., Spinks, G.M., Whitten, P.G., 2011. Progress toward robust polymer hydrogels. Aust. J. Chem. 64 (8), 1007–1025.

Noori, S., Kokabi, M., Hassan, Z.M., 2015. Nanoclay enhanced the mechanical properties of poly(vinyl alcohol)/chitosan/montmorillonite nanocomposite hydrogel as wound dressing. Procedia Mater. Sci. 11, 152–156.

Prentice, P., 1995. Rheology and its Role in Plastics Processing, 84. iSmithers Rapra Publishing.

Saghafi, H.R., Emadi, M.A., Farasat, A., Arabloo, M., Naderifar, A., 2016a. Performance evaluation of optimized preformed particle gel (PPG) in porous media. Chem. Eng. Res. Des. 112, 175–189.

Saghafi, H.R., Naderifar, A., Gerami, S., Emadi, M.A., 2016b. Improvement in thermo-chemical stability of nanocomposite preformed particle gels for conformance control in harsh oil reservoir conditions. Can. J. Chem. Eng. 94 (10), 1880–1890.
Saghafi, H.R., Naderifar, A., Gerami, S., Farasat, A., 2016c. Performance evaluation of viscosity characteristics of enhanced preformed particle gels (PPGs). Iran. J. Chem. Chem. Eng. (IJCCE) 35 (3), 83–92.
Sang, Q., Li, Y., Yu, L., Li, Z., Dong, M., 2014. Enhanced oil recovery by branched-preformed particle gel injection in parallel-sandpack models. Fuel 136, 295–306.
Sorbie, K.S., 2013. Polymer-improved Oil Recovery. Springer Science & Business Media.
Spildo, K., Skauge, A., Skauge, T., 2010. Propagation of colloidal dispersion gels (CDG) in laboratory corefloods. In: SPE Improved Oil Recovery Symposium. Society of Petroleum Engineers.
Tang, H., 2007. Preformed Particle Gel for Conformance Control in an Oil Reservoir. Google Patents.
Tongwa, P., Bai, B., 2014. Degradable nanocomposite preformed particle gel for chemical enhanced oil recovery applications. J. Petroleum Sci. Eng. 124, 35–45.
Van Vliet, T., Van Dijk, H., Zoon, P., Walstra, P., 1991. Relation between syneresis and rheological properties of particle gels. Colloid Polym. Sci. 269 (6), 620–627.
Wang, J., Liu, H.-q., Wang, Z.-l., Hou, P.-c, 2012. Experimental investigation on the filtering flow law of pre-gelled particle in porous media. Transp. Porous Med. 94 (1), 69–86.
Wang, J., Liu, H., Wang, Z., Xu, J., Yuan, D., 2013. Numerical simulation of preformed particle gel flooding for enhancing oil recovery. J. Petroleum Sci. Eng. 112, 248–257.
Wu, Y.-S., Bai, B., 2008. Modeling particle gel propagation in porous media. In: SPE Annual Technical Conference and Exhibition. Society of Petroleum Engineers.
Yao, C., Lei, G., Li, L., Gao, X., 2012. Selectivity of pore-scale elastic microspheres as a novel profile control and oil displacement agent. Energy & Fuels 26 (8), 5092–5101.
Yu, Y., Zhu, C., Liu, Y., Zhang, E., Kong, Y., 2011. Synthesis and characterization of N-maleyl chitosan-cross-linked poly(acrylamide)/montmorillonite nanocomposite hydrogels. Polymer-Plastics Technol. Eng. 50 (5), 525–529.
Zamani, A., Maini, B., 2009. Flow of dispersed particles through porous media — deep bed filtration. J. Petroleum Sci. Eng. 69 (1–2), 71–88.
Zhang, H., 2014. Preformed Particle Gel Transport through Fractures. Doctoral Dissertations. Missouri University of Science and Technology.
Zhang, H., Challa, R.S., Bai, B., Tang, X., Wang, J., 2010. Using screening test results to predict the effective viscosity of swollen superabsorbent polymer particles extrusion through an open fracture. Industrial Eng. Chem. Res. 49 (23), 12284–12293.
Zhang, H., et al., 2016. Molecular dynamics study on mechanism of preformed particle gel transporting through nanopores: surface hydration. RSC Adv. 6 (9), 7172–7180.